MENTORSHIP, SCHOLARSHIP, AND SERVICE: A SPECIAL ISSUE HONOURING PROFESSOR ADAMU N. BABA-KUTIGI, FNIP ON HIS RETIREMENT
FUDMA Journal of Sciences (FJS)
ISSN online: 2616-1370
ISSN print: 2645 - 2944
Vol. 10 ANB-K Special Issue, 2026, pp 96 – 105
DOI: https://doi.org/10.33003/fjs-2026-10(ANB-K)-5321

First-Principles Investigation of the Electronic and Optical Properties of Tin Chalcogenides (SnS, SnSe and SnTe) Using Density Functional Theory

***[1,2]Salihu Ibrahim Kagara, [1]Abubakar Yakubu, [1]Yahaya Abubakar Aliero, [1]Sirajo Abdullahi**

[1]Department of Physics, Faculty of Physical Science, Abdullahi Fodio University of Science and Technology Aliero, Kebbi State, Nigeria.
[2]Department of Science Education, Faculty of Education, Zamfara state university Talata Mafara, ZAMSUT. Zamfara State, Nigeria.

*Corresponding authors' email: Salihukagara011@gmail.com Phone No: 08161823738

ABSTRACT

We have studied the electrical and optical properties of SnA (A = S, Se, Te) through first-principles calculations within Density Functional Theory (DFT) as implemented in Quantum ESPRESSO. The Generalised Gradient Approximation (GGA) was exchange-correlation is used in form of Perdew-Burke-Ernzerhof (PBE) and Perdew-Burke-Ernzerhof for solids (PBESol). The study shows different trends in the electronic behaviour of the Chalcogenides: SnS is a semiconductor with a low direct band gap (0.186 and 0.087 eV for both PBE and PBESol) while SnSe and SnTe have metallic behaviours with zero band gap this could be due to the well-known underestimation of band gaps by standard GGA approximations and the lack of spin-orbit coupling effects. The optical properties such as complex dielectric function, refractive index, absorption coefficient, energy loss function, extension coefficient and reflectivity are calculated. The peak of the dielectric function is red shifted from SnS to SnTe.

The SnS refractive index with PBE has high static values (n = 3.3). The onset of the PBE optical absorption is at around 1.5 eV for SnS and 1.0 eV for SnTe. The energy loss function of SnTe exhibits a strong plasmon peak and good optical conductivity. The results show a consistent red-shift in the absorption edges and improvement in optical conductivity from SnS to SnTe compared to the decrease in band gap. SnSe and SnTe have a very strong metallic-like optical response which suggest the possibility for infrared optoelectronic devices whereas SnS shows promising absorption in the visible to infrared region suitable for photovoltaic applications. This comparative study gives important guidance for optoelectronic technologies through theoretical insights into the properties of tin chalcogenides.

Keywords: Tin Chalcogenides, Density Functional Theory, Band Gap, Photovoltaic Materials, Infrared Optoelectronics

INTRODUCTION

The global demand for renewable energy and improved energy efficiency is increasing, driven by the finite availability of non-renewable resources like fossil fuels. Meeting this demand requires technological innovation, particularly in fields such as photovoltaics (PV) and thermoelectrics (TE) (International Energy Agency, 2023). In addition to silicon, research has focused on various materials for solar energy conversion, including sulfides, selenides, tellurides, perovskites, oxides, and organic compounds. Among these, chalcogenides—chemical compounds containing at least one chalcogen anion (group 16 elements) and one or more electropositive elements—have attracted significant interest. Tin chalcogenides, composed of tin (Sn) and a chalcogen such as sulfur (S), selenium (Se), or tellurium (Te), generally adopt an A–X formula (where A is a metal, Sn, and X is a chalcogen). These materials often exhibit layered or framework structures, along with adjustable band gaps, thermal stability, and advantageous charge transport properties (Pandit and Hamad, 2021).

Previous studies on thermoelectric and optoelectronic materials have examined various tin chalcogenides, including monolayers such as SnX (X=Se, S), two-dimensional SnX (X=Te, S), SnTe, SnS, SnSe, SnTe-based compounds, ternary chalcogenides like XIn_2S_4 (X=Zn, Cd, Hg), $AlAuO_2$, $AlAu_{0.94}Fe_{0.06}O_2$, and double perovskites such as Rb_2SeX_6 (X=Cl, Br). Among these, SnSe and SnTe have been identified as particularly promising for thermoelectric applications, while SnS shows potential for optoelectronic uses (Fatahi et al., 2020; Rundle and Leon, 2022). Specifically, SnSe and SnTe possess distinctive electronic band structures, featuring regions of both high and low dispersion in the Brillouin zone. These characteristics, combined with significant acoustic-optical phonon interactions, make them strong candidates for thermoelectric devices (More et al., 2023).

Thermoelectric properties of Tin-chalcogenides SnX (X = Te, Se and S) are studied by Dong *et al.*, (2019) using USPEX and VASP. They found SnX (X = Te, Se, and S) (β′ phase) suitable for thermoelectric applications using GGA as an exchange correlation functional. Bafekry *et al.,* (2021) also studied the electronic, optical, mechanical and properties of semiconducting chalcogenide alloys (Ge, Sn, Pb) (S,Se, Te) using PBE and HSE06 exchange correlation functionals using spin orbit coupling with the VASP . They found that the alloys being studied have good optical and mechanical properties, and are semi-conductors.

Despite their promise, SnA compounds (where A = S, Se, Te) have not been extensively investigated using a unified first-principles methodology. A significant research gap remains regarding the integrated analysis of their structural, electronic, optical, mechanical, and thermoelectric properties.

In this work, the optoelectronic properties of tin chalcogenides SnA (A = S, Se and Te) are studied by using DFT as implemented Quantum ESPRESSO algorithm. The

exchange correlation functionals used in this study are GGA-PBE and GGA-PBESol. No work has been done so far, to our knowledge, on the opto-electronic properties of tin chalcogenides SnA (A = S, Se, and Te) by using GGA-PBE and GGA-PBESol exchange correlation functionals. The manuscript is organised as follows: in section two we describe the computational details, in section three we discuss the obtained results and in section four we present the conclusions of the work.

MATERIALS AND METHODS

Computational Details

The electronic and optical properties of tin chalcogenide (SnA, where A = S, Se, Te) were calculated using the Quantum ESPRESSO code (Giannozzi *et al.,* 2009). A plane-wave basis set was employed to represent electron wavefunctions. Electron-ion interactions was described using norm-conserving pseudopotentials, and the exchange-correlation functionals used was Generalized Gradient Approximation (GGA) in both the Perdew–Burke–Ernzerhof (PBE) and Perdew–Burke–Ernzerhof for solids (PBESol) (Perdew *et al.,* 1992; Perdew *et al.,* 1996).

SnS and SnSe have a space group of Pnma with orthorhombic crystal structure while SnTe have a space group of Fm-3m with a cubic crystal structure. Lattice Parameters for SnS and SnSe are a ≈ 4.33 Å, b ≈ 11.19 Å, c ≈ 3.98 Å and a ≈ 4.15 Å, b ≈ 11.50 Å, c ≈ 4.44 Å respectively. While SnTe have a Lattice Parameters of a ≈ 6.32 Å. The calculations used a kinetic energy cut-off of 100 Ry and a 6 × 6 × 6 k-point mesh for Brillouin zone integration. A plane-wave cut-off of 120 Ry, energy convergence criterion of 10^{-5} eV, and a force convergence threshold of 10^{-5} eV/Å were used during structural optimization. A Γ-centered 6 × 6 × 6 k-mesh was used for geometry relaxation, band structure and optical properties calculations. Denser k-point meshes of 12 × 12 × 12 and 32 × 32 × 32 were used for computing the Density of States (DOS) and Projected Density of States (PDOS), respectively. Structural relaxation was performed using the BFGS (Broyden-Fletcher-Goldfarb-Shanno) quasi-Newton algorithm (Broyden, 1970(a); Broyden, 1970(b)), and atomic positions were fully optimized for subsequent DOS, PDOS, and optical property calculations.

The complex dielectric function, $\varepsilon(\omega) = \varepsilon_1(\omega) + i\varepsilon_2(\omega)$, describes the macroscopic optical response. The imaginary part ($\varepsilon_2(\omega)$) was determined directly from the momentum matrix elements between occupied and unoccupied electronic states. The real part ($\varepsilon_1(\omega)$) was then derived from the imaginary part using the Kramers-Kronig relations (Artoni and La Rocca, 2015).

$$\varepsilon_1(\omega) = \frac{2}{\pi}\rho \int_o^{\infty} \frac{\omega'^2 \varepsilon_2 \omega}{\omega'^2 - \omega^2} \quad (1)$$

$$\varepsilon_2(\omega) = \frac{-2}{\pi}\rho \int_o^{\infty} \frac{\omega'^2 \varepsilon_2 \omega}{\omega'^2 - \omega^2} \quad (2)$$

The optical properties were studied for SnS, SnSe, SnTe by utilizing the real and imaginary parts of the dielectric function. Other optical parameters considered include: refractive index (n (ω)), reflectivity (R (ω)), conductivity (Re (σ)), energy-loss functions (L (ω)), extinction coefficient (K (ω)), and absorption coefficient (I (ω)). The following expressions are utilized in their computation:

$$n(\omega) = \sqrt{\frac{|\varepsilon(\omega)| + \varepsilon_1(\omega)}{2}}, \quad (3)$$

$$\mathrm{R}(\omega) = \frac{(n-1)^2 + k^2}{(n+1)^2 + k^2}, \quad (4)$$

$$\mathrm{Re}(\sigma) = \frac{\omega}{4\pi}\,\varepsilon_2(\omega), \quad (5)$$

$$\mathrm{I}(\omega) = \sqrt{2\omega}\left(\frac{\varepsilon_1(\omega)^2 + \varepsilon_2(\omega)^2 = \varepsilon_1(\omega)}{2}\right), {}^{1}/_{2} \quad (6)$$

$$\mathrm{L}(\omega) = \frac{\varepsilon_1}{\varepsilon_1^2 + \varepsilon_2^2}, \quad (7)$$

$$\mathrm{RE} = \frac{nE - 1^2 + K^2}{nE + 1^2 + K^2} \quad (8)$$

$$\mathrm{K}(\omega) = \sqrt{\frac{|\varepsilon(\omega)| - \varepsilon_1(\omega)}{2}}, \quad (9)$$

RESULTS AND DISCUSSION

Electronic Properties

The electronic properties of SnS, SnSe, and SnTe were analyzed based on their calculated energy band structures, total density of states (TDOS), and partial density of states (PDOS). These properties were computed using the Generalized Gradient Approximation with the Perdew-Burke-Ernzerhof (GGA-PBE) and the Perdew-Burke-Ernzerhof for solids (PBESol) functionals to model exchange-correlation effects.

Band Structure

The electronic band structures for SnS, SnSe, and SnTe were determined at their equilibrium volumes along high-symmetry directions within the first Brillouin zone. The results, calculated with both the GGA-PBE and GGA-PBESol functionals, are presented in Figures 1–3. Additionally, the corresponding total and partial density of states for these chalcogenides are shown in Figures 4–9.

Table 1: Band Gap Values Of Tin Chalcogenides Compound Sna (A = S, Se, and Te)

Tin Chalcogenide	EXC	BAND (eV)
SnS	GGA-PBE	0.1859
	GGA-PBESol	0.0865
SnSe	GGA-PBE	0.0000
	GGA-PBESol	0.0000
SnTe	GGA-PBE	0.0000
	GGA-PBESol	0.0000

The data presented in Table 1 indicates that SnS possesses a small band gap of 0.185 eV (PBE) and 0.086 eV (PBESol), classifying it as a narrow-band-gap semiconductor bordering on semi metallic behavior as illustrated in figure 1. In contrast, both SnSe and SnTe exhibit a zero band gap across both functionals, as illustrated in Figures 2 and 3, this could be due to the well-known underestimation of band gaps by standard GGA approximations and the lack of spin-orbit coupling effects, signifying metallic characteristics. In these compounds, the valence band maximum (VBM) and conduction band minimum (CBM) overlap at Fermi level. A clear trend emerges where the calculated band gap diminishes across the series S → Se → Te. SnS retains a small gap, while SnSe and SnTe become gapless. This progression correlates with the increasing atomic mass, relativistic effects, and size of the chalcogen atom, accompanied by a decrease in electronegativity. (Batool *et al.,* 2022). This computational trend aligns with experimental observations, where heavier chalcogenides generally exhibit smaller bandgaps, with reported values for SnS (0.95–1.37 eV) and SnSe (0.89–1.20

eV) (Malon and Kaxiras, 2013; Fernandes *et al*., 2013). The small band gap makes SnS suitable for applications such as photovoltaic or infrared detectors, where narrow-gap semiconductors are desirable. However for SnSe and SnTe their metallic nature suggests better use as metal compounds, where high carrier mobility and overlapping bands are useful. These trends suggest that SnS is more suitable for optoelectronic applications, while SnSe and SnTe remain attractive for metalic applications.

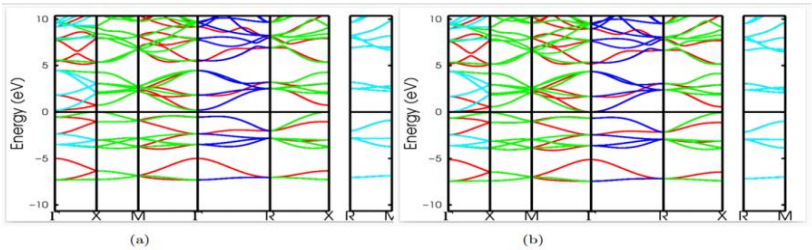

Figure 1: Plots of Band Structure for SnS Calculated using (a) GGA-PBE (b) GGA-PBESol

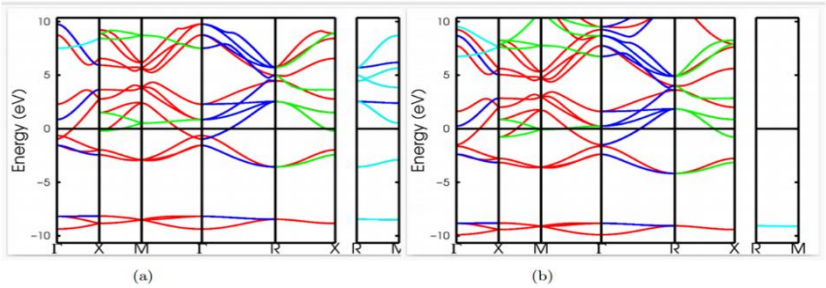

Figure 2: Plots of Band Structure for SnSe Calculated using (a) GGA-PBE (b) GGA-PBESol

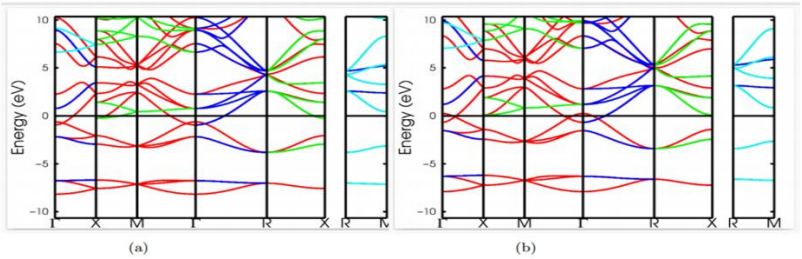

Figure 3: Plots of Band Structure for SnTe Calculated using (a) GGA-PBE (b) GGA-PBESol

Total Density of State (TDOS) and Partial Density of State (PDOS)

The density of states (DOS) offers insight into electronic transitions between the valence and conduction bands, revealing the distribution of electronic orbitals across a range of energies within the band structure (Adewale *et al.*, 2021). Calculated TDOS and PDOS plots for the tin chalcogenides SnA (A = S, Se, Te), obtained using both GGA-PBE and GGA-PBESol functionals, are presented in Figures 4–9.

The results reveals that, for SnS under both functionals, the DOS does not cross the Fermi level (E_F) as shown in Figure 4. This confirms the semiconducting nature of SnS. In contrast, the DOS plots for both SnSe and SnTe show a distinct crossing of electronic states at the Fermi level for each functional as shown in Figures 5 and 6. This characteristic indicates that these compounds exhibit metallic behavior as indicate in the band structure result.

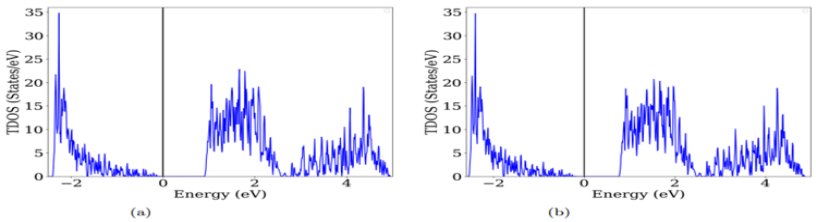

Figure 4: Plots of TDOS for SnS Calculated using (a) GGA-PBE (b) GGA-PBESol

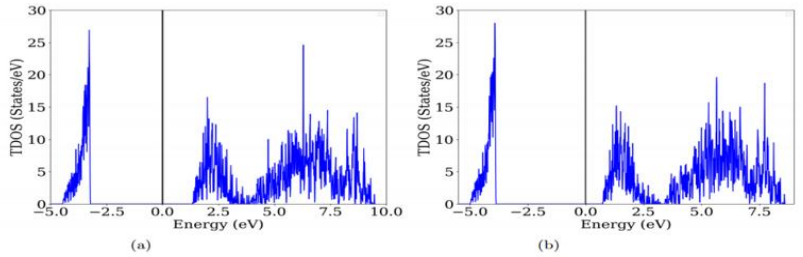

Figure 5: Plots of TDOS for SnSe Calculated using (a) GGA-PBE (b) GGA-PBESol

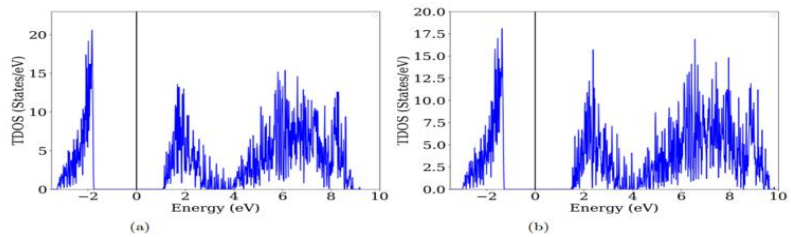

Figure 6: Plots of TDOS for SnTe Calculated using (a) GGA-PBE (b) GGA-PBESol

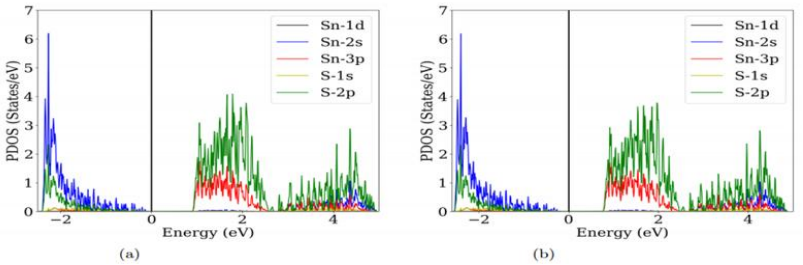

Figure 7: Plots of PDOS for SnS Calculated using (a) GGA-PBE (b) GGA-PBESol

Figure 7 (a) shows the Partial density of states (PDOS) for SnS, calculated using GGA-PBE functional, the figure described SnS compound with semiconducting character, with valence band maximum (VBM) around ~0 eV and the conduction band minimum (CBM) start just above it. The valence band, crossing from approximately -5 eV to the Fermi level, displays a multi-peak structure showing a strong orbital hybridization between Sn and S atoms. This electronic structure confirms the material's potential for optoelectronic applications. While figure 7 (b) shows the PDOS for SnS calculated using the GGA-PBESol functional which confirms the semiconducting nature of the compound, exhibiting a direct band gap. The valence band, characterized by a complex multi peak structure showing that SnS orbital hybridization is strong. This result further validates the appropriateness of SnS for optoelectronic applications.

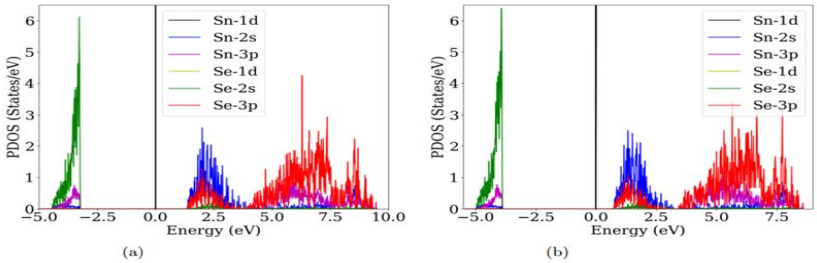

Figure 8: Plots of PDOS for SnSe Calculated using (a) GGA-PBE (b) GGA-PBESol.

Figure 8 (a) described the PDOS plot for SnSe, calculated using the GGA-PBE functional, which shows metallic nature of the compound with a band gap of approximately 0 eV. This electronic structure strengthens SnSe suitability for applications in infrared optoelectronics. Figure 8 (b) demonstrates PDOS plot for SnSe, calculated using the PBESol functional, the figure described semiconducting nature for SnSe compound with a direct band gap of approximately 0.0 eV. The conduction band, start from the conduction band minimum of ~0.0 eV and extending to approximately 6 eV, is predominantly comprised of Sn-5p character. GGA-PBEsol-calculated band gap of ~0.0 eV is notably the same with standard GGA-PBE functional (~0.0 eV).

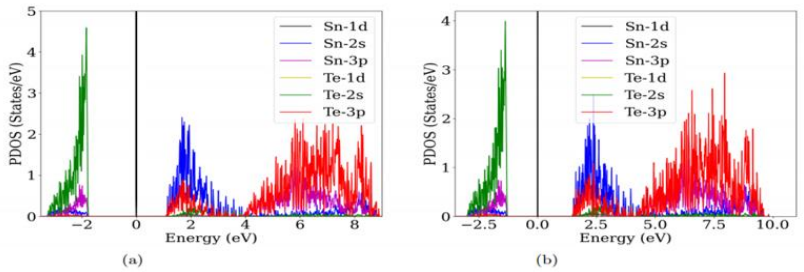

Figure 9: Plots of PDOS for SnTe Calculated using (a) GGA-PBE (b) GGA-PBESol

Partial density of states plot for SnTe calculated using the GGA-PBE functional identifies the metallic behaviors of SnTe compound notable by a finite density of states at the Fermi energy level as shown in Figure 9 (a). The valence band, starting from approximately -8 eV to the Fermi energy level, is formed by hybridized Sn-p and Te-p orbitals. This absence of a band gap, in stark contrast to the semiconducting nature of SnS, conclusively classifies SnTe as a metal like it indicates in the band structure results. While figure 9(b) shows the plot PDOS for SnTe calculated using the PBESol functional, which confirms the metallic behavior of SnTe. The valence band, characterized by a structured density of states derived from hybridized Sn-p and Te-p orbitals, starting from approximately -6 eV and crosses continuously through the Fermi energy level into the conduction band.

Optical Properties

Optical properties of Sn-chalcogenides was studied to understand the light-matter interaction. Considering the significance of lower dimensionality and the influence of anisotropy, the optical properties can be described mathematically by a complex dielectric function $\varepsilon(\omega)$; expressed as $\varepsilon(\omega)=\varepsilon_1(\omega)+\varepsilon_2(\omega)$, where $\varepsilon_1(\omega)$ and $\varepsilon_2(\omega)$ indicate the real and imaginary parts associated with the band structure (Nwachuku, 2025). It can be determined by considering all transitions between occupied and unoccupied electronic states. In order to relate the real and imaginary parts, the Kramer's- Kronig transformation were used (equations (1) and (2)). Other optical properties like refractive index (n), reflectivity R(ω) optical conductivity (σ), absorption coefficient (α), Energy loss function L(ω), and extension coefficient K(ω) are calculated using equations (3) – (9) respectively.

Dielectric Function

Both real and imaginary components of the dielectric function ($\varepsilon_1(\omega)$ & $\varepsilon_2(\omega)$) hold information regarding the optical behavior of the medium and the excitations of phonons occurring from their interaction with photons (Nwachuku, 2025). Figures 10 and 11 shows the plots of real and imaginary dielectric function for the studied tin chalcogenides compound SnA (A = S, Se, Te), the dielectric functions are plotted over the photon energy range of (0 - 30 eV) using both PBE-GGA and GGA-PBESol.

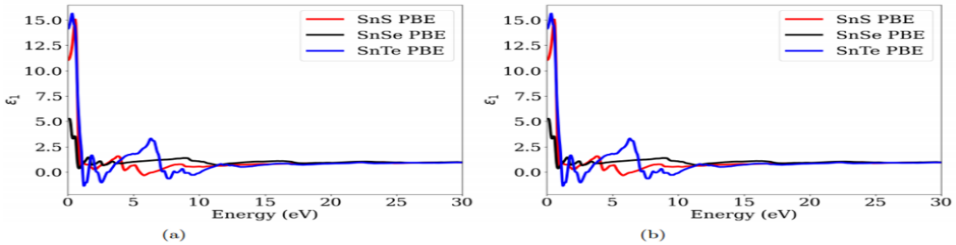

Figure 10: Plots of Real Dielectric Function for SnA Calculated using (a) GGA-PBE and (b) GGA-PBESol

Figure 10 (a) shows the real part of dielectric function ($\varepsilon_1(\omega)$) computed using GGA-PBE, from the plots, SnS have $\varepsilon_1(\omega) \approx 16$ with the maximum peak at around 1.5 eV and SnSe has $\varepsilon_1(\omega) \approx 4.8$ with peak near 1.3 eV while SnTe have $\varepsilon_1(\omega) \approx 13.5$ at around to 1.1 eV. However, figure 10 (b) shows the plot of real part of dielectric function ($\varepsilon_1(\omega)$) computed using GGA-PBESol, from the figure, $\varepsilon_1(\omega) \approx 15$, for SnS at around 1.2 eV, SnSe have $\varepsilon_1(\omega) \approx 35$ eV at around 1 eV while SnTe have $\varepsilon_1(\omega) \approx 75$ at around 0.8 eV.

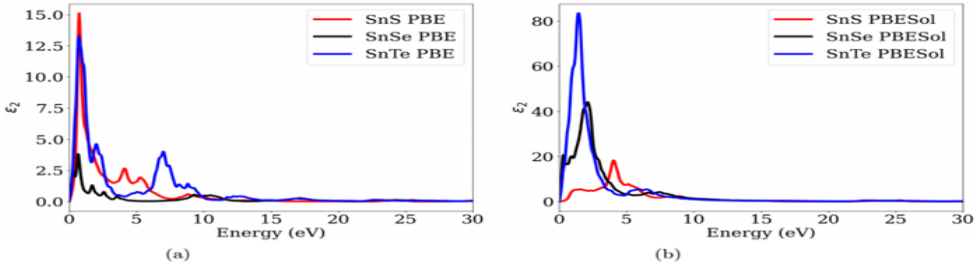

Figure 11: Plots of Imaginary Dielectric Function for SnA Calculated using (a) GGA-PBE and (b) GGA-PBESol

The result of the real part of the dielectric function clearly demonstrates the enhancement of the optical polarisation strength when the chalcogen atom is changed from S to Te. The strongest dielectric response is found for SnTe among the

studied compounds, particularly in the GGA-PBESol approximation, which suggests its high sensitivity to external electric fields. SnSe is intermediate between SnS and SnTe, which has a moderate response. The dielectric behaviour shows slow increase from SnS to SnTe indicating the enhancement of electronic polarisability and decrease of resistance to electric field distortion through the addition of heavier chalcogen atom. SnTe is the most promising material for high end dielectric and optoelectronic applications.

The result of imaginary part of dielectric function ($\varepsilon_2(\omega)$) for GGA-PBE are shown in Figure 11 (a). From the figure, the SnS have $\varepsilon_2(\omega) \approx 16$ at around 2.0 eV, SnSe have $\varepsilon_2(\omega) \approx 4.8$ with at around 1.8 eV and SnTe have $\varepsilon_2(\omega) \approx 13.5$ at around 1.2 eV. The result of imaginary part of dielectric function ($\varepsilon_2(\omega)$) for GGA-PBESol is shown in Figure 11 (b). From the figure, SnS have $\varepsilon_2(\omega) \approx 18$ at around 1.8 eV, SnSe have $\varepsilon_2(\omega) \approx 42$ at around 2.5 eV and SnTe have $\varepsilon_2(\omega)$ at $\approx$ 84 at around 4.5 eV. E2 arises from inter band transitions. The main peak shows the onset of optical activity. The red shift (toward lower energy) from SnS to SnTe which reflects band gap narrowing.

The imaginary part of the dielectric function indicates an increasing optical transition strength with increasing chalcogen atomic mass. Optical activity is most prominent in SnTe, with enhanced interband electronic transitions at lower photon energy, whereas SnS shows comparatively weaker behaviour. SnSe has intermediate properties between the two compounds. The large red shift from SnS, SnSe to SnTe confirms gradual reduction in band gap and indicates enhanced interaction between electromagnetic radiation and electronic structure of the materials. Such behaviour shows SnTe as a better optical material for low energy optoelectronic applications.

Refractive Index

The refractive index n (ω) of a material is simply the ratio of the speed of light in free space to the speed of light in a given material (Rahman *et al*., 2023). Figure 12 show the refractive index variation against photon energy for SnA (A = S, Se, Te) compounds. From te plots, SnS have n (w) $\approx$ 3.3 at around $\approx$ 1.8 eV, SnSe have n (w) $\approx$ 2.3 at around 1.3 eV and SnTe have n (w) $\approx$ 3.8 at around 1.1 eV. Refractive index identify that, the static refractive index (n_o) follows the order SnS > SnSe consistent with bandgap trend (E_g(SnS) > E_g(SnSe and SnTe).

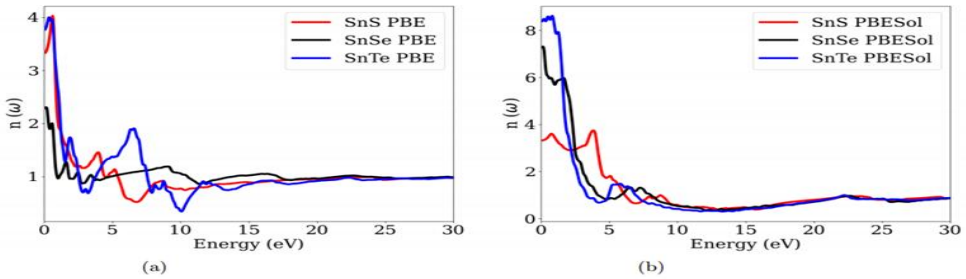

Figure 12: Plots of Refractive Index for SnA Calculated using (a) GGA-PBE and (b) GGA-PBESol

The refractive index results show large differences in the light propagation in the tin chalcogenides. SnTe has the highest refractive index indicating stronger polarisation effects and denser electronic environment near the Fermi level. SnS has also shown relatively high refractive characteristics, where SnSe has the lowest values among the studied compounds. In all the cases the refractive index decreases with increasing of photon energy confirming normal dispersion characteristics. The overall improved refractive behaviour of SnTe indicates a better light confinement and stronger optical interaction as compared to SnS and SnSe. High values of refractive index with lower photon energy indicates a very strong polarization and denser electronic states near the Fermi energy level. As the energy increases refractive index will decrease showing normal dispersion beyond the fundamental absorption edge (Batool *et al*., 2022).

Reflectivity

Reflectivity is one of the good properties of the optoelectronics materials, materials with higher reflectivity have higher solar reflectance. SnA (A= S, Se, and Te) optical reflectivity was calculated from dielectric constant (Adewale *et al*, 2023). Materials' morphology is determined by light reflection, which indicates surface roughness (Yahaya *et al*., 2024). The plots of optical reflectivity against the photon energy (0-30 eV) was presented in Figure 13.

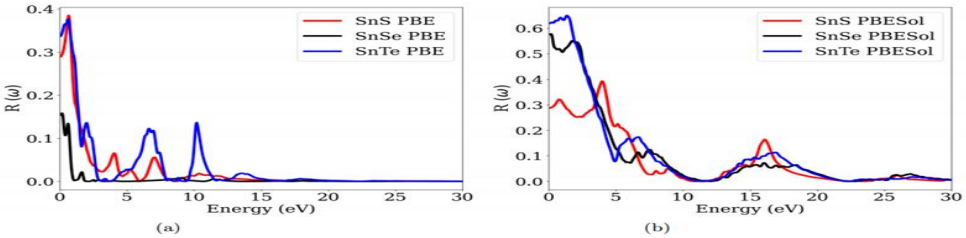

Figure 13: Plots of Optical Reflectivity for SnA Calculated using (a) GGA-PBE and (b) GGA-PBESol

From the plots, SnS have R = 0.47 at around 3.3 eV, SnSe have R = 0.17 at around 2.7 eV and SnTe have R= 0.48 at around 2.2 eV. The results from the plots shows that, reflectivity peaks coincides with inter band transition energies, in which the photons excite electrons from the valance band to the conduction band. The reflectivity spectra reveal that SnTe and SnS have much higher reflectance than SnSe. SnTe shows the most pronounced metallic-like optical behaviour, due to its smaller band gap and the effect of the heavier tellurium atom. The higher reflectivity values are

correlated with stronger electronic transitions between valence and conduction bands. On the other hand, SnSe has relatively low reflectivity, which indicates a weaker surface optical response. The overall results indicate that SnTe is more suitable for applications with high optical reflectance and infrared response enhancement. The higher reflectivity in SnTe indicates stronger metallic like response, consistent with its smaller band gap and heavier anion (Te). At photon energies > 5 eV reflectivity fall off due to the reduced electronic transition probability (Batool *et al*, 2022).

Optical Conductivity

The optical conductivity calculations can reveal whether the materials can be exploited in opto-electronics applications (Yahaya *et al*., 2024). The conductivity plots of SnS, SnSe, and SnTe are shown in Figure 14 computed using both GGA-PBE and GGA-PBESol. The figure reveals that the conductivity of SnTe computed using GGA-PBE is slightly greater than that of SnS, and SnSe, within the energy level of around 1.1 eV, 1.2 eV, and 7.2 eV respectively, with high peak of ≈ 0.18 for SnTe, 0.065 for SnS and 0.015 for SnSe. However for GGA-PBESol the conductivity of SnTe is slightly greater than that of SnSe and SnS within the energy range of around 1.8 eV, 2.2 eV, and 4.9 eV respectively. The peak conductivity at these energy range are 0.72 (SnTe), 0.56 (SnSe) and 0.44 (SnS) respectively.

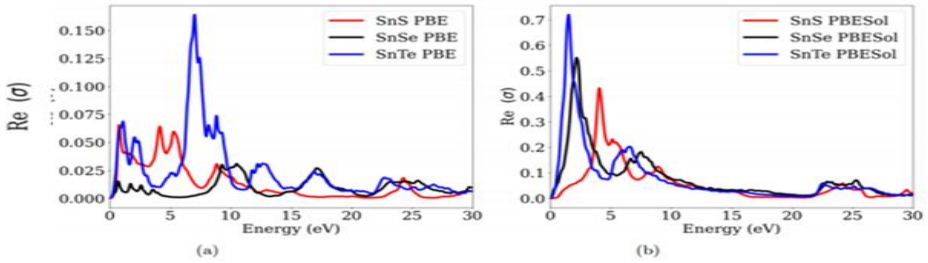

Figure 14: Plots of Optical Conductivity for SnA Calculated using (a) GGA-PBE and (b) GGA-PBESol

The optical conductivity calculations show a clear increase in conductivity from SnS to SnTe for GGA-PBE and GGA-PBESol functionals. SnTe always presents the highest peaks of conductivity, which means that under the photon irradiation it has the strongest excitation of charge carriers and the greatest electronic mobility. SnSe has moderate conductivity values and SnS has the lowest values. The enhanced optical conductivity of SnTe confirms the superior potential for the optoelectronic and photoconductive device applications where efficient charge transport is essential.

Absorption Coefficient

The absorption coefficient is calculated to visualize the absorptive nature of considered materials under the influence of incident photons passing through particular material (Alzahrani *et al*., 2021).

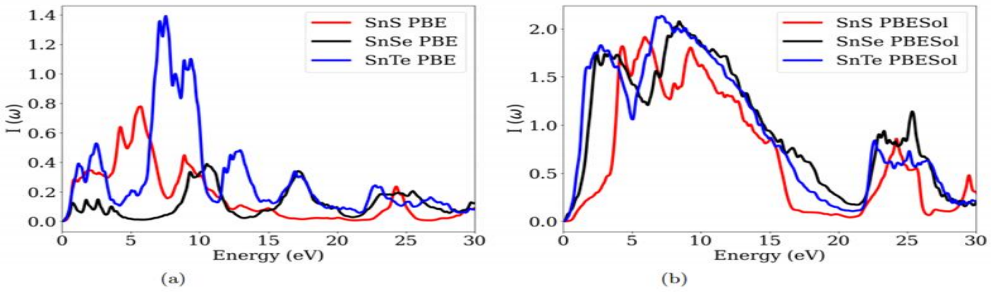

Figure 15: Plots of Absorption coefficients for SnA calculated using (a) GGA-PBE and (b) GGA-PBESol

Figure 15 shows the plots of absorption coefficient spectra of SnS, SnSe, and SnTe, calculated using both PBE and PBESol functionals, identifying the optical transition behavior of the tin chalcogens compound. Figure 15 (a) described that I (w) calculated using GGA-PBE, the absorption begin at ~1.5 eV for SnS, ~1.2 eV for SnSe, and ~1.0 eV for SnTe, while that of figure 15 (b) (I (w) calculated using GGA-PBESol) start at 6 eV for SnS, ~8 eV for SnSe, and ~7 eV for SnTe showing reduction in band gap with increasing chalcogen atomic mass. The results revealed that SnTe demonstrate stronger electron–photon interaction and higher free-electron density. The overall increase in peak intensity and red-shift in absorption edge from SnS → SnSe → SnTe identified the light absorption capability and reduced band gap with heavier chalcogen atoms. These results demonstrate that, SnTe have the highest optical activity, making it more applicable for visible and infrared optoelectronic applications, while SnS and SnSe maintain strong absorption in the lower energy region, making it useful for solar energy conversion and photovoltaic devices.

Electron Energy Loss Function

The energy-loss function L is related to the energy loss of very fast moving electrons crossing the material, it is a very important optical parameter and also related to the imaginary part of complex dielectric function (Rahman *et al*., 2023). Figure 16 (a) and (b), the electron energy loss function (EELF) spectra of SnS, SnSe, and SnTe shows clear differences in plasmatic behavior across the compound. Figure 16 (a), SnS shows its main Plasmon peak around 8.5 eV, SnSe around 10 eV, and SnTe around 10.5 eV, with the latter exhibiting the strong and sharp resonance. While in figure 16 (b), SnS shows its main plasmon peak around 15.5 e, SnSe around 15 eV, and SnTe around 14.5 eV, with the

latter exhibiting the most strong and sharp resonance. This indicates a progressive increase in plasmon energy, free-electron density, and metallic character from SnS to SnTe. The electron energy-loss analysis reveals a progressive enhancement of the plasmonic features and free-electron character from SnS to SnTe. SnTe shows the sharpest and most intense plasmon resonance peaks, indicating a stronger collective oscillation of electrons and better metallic properties. SnSe exhibits intermediate plasmonic behavior, while SnS exhibits relatively weak resonance features. The results indicate that SnTe has the largest free-electron density and the strongest response of electronic excitation among the tin chalcogenides studied.

Extinction Coefficient

The extinction coefficient, K(ω), is one of the important physical characteristic related to a material's ability to absorb light at a specific frequency that defines electromagnetic waves' movement through any medium (Nabi and Gupta, 2021).

Figure 17 (a) and (b) illustrates the plots of the extinction coefficient (K (ω)) for SnS, SnSe, and SnTe, calculated using the GGA-PBE and PBESol functionals. In figure 17 (a), the absorption onset, marking the material's band gap, shifts to lower energies from SnS (starting around ~1.5 eV) to SnSe (~1.0 eV) to SnTe (near 0.0 eV). The first major peak in K (ω) also follows this trend, appearing at approximately 7-8 eV for SnS (K ~2.0), red shifted to ~6-7 eV for SnSe (K >2.0), also to ~5-6 eV for SnTe. A second prominent peak is observed around 12-13 eV for SnS (K ~1.7), which broadens and shifts in SnSe and SnTe. And figure 17 (b) the absorption onset with higher peak point for SnS of 2.8 at ~ 4.8 eV and shifted to the lower peak point of 0.3 at 26 eV, SnSe has the higher peak of 5.0 at 3.5 eV and shifted to a lower peak of 0.4 at 22.5 eV, while SnTe has the higher peak of 6.7 at 2.2 eV with lower peak of 0.4 at 22.5 eV.

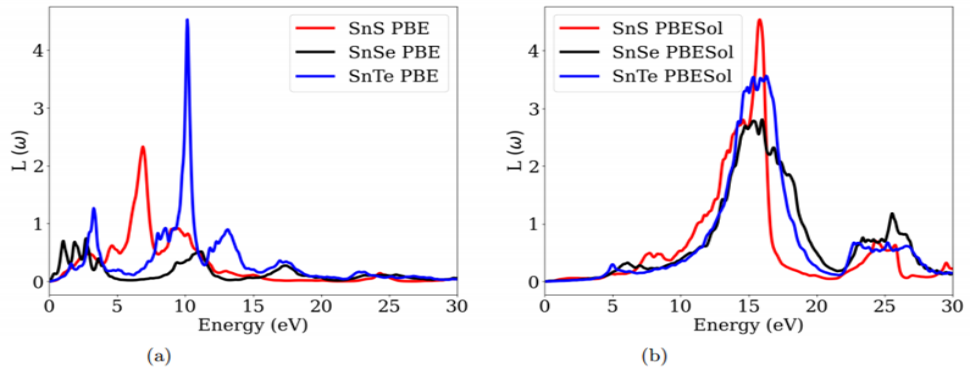

Figure 16: Plots Of Electron Energy Loss Function for SnA Calculated using (a) GGA-PBE and (b) GGA-PBESol

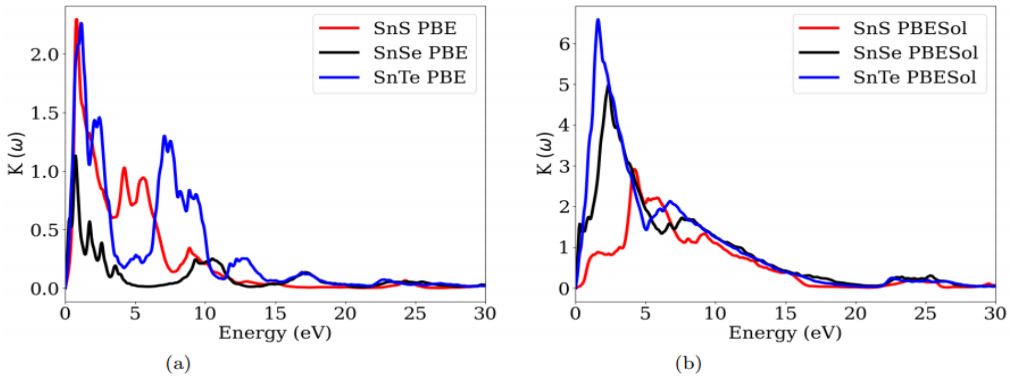

Figure 17: Plots of Extinction Coefficients for SnA Calculated using (a) GGA-PBE and (b) GGA-PBESol

This systematic progression where spectra red shift, peak magnitudes increase, while the features broaden demonstrates how the decreasing band gap and strengthening spin-orbit coupling from the sulfide to the telluride enhance absorption intensity at lower energies.

The results of extinction coefficient further confirm the improved optical absorption characteristics as the chalcogen element varies from S to Te. SnTe has the highest extinction coefficient with absorption at lower photon energies showing better attenuation of electromagnetic waves. The extinction behavior of SnSe is moderate. However, SnS shows relatively smaller peak intensities. The gradual red shift and the enhanced peak broadening from SnS to SnTe are proof for effect of band gap reduction and stronger spin-orbit coupling effects. Therefore, SnTe exhibits the best overall optical absorption performance among the studied compounds.

CONCLUSION

The electronic and optical properties of Tin chalcogenide SnA (A=S, Se and Te) have been successfully studied in this work by first-principles calculations based on the Density Functional Theory (DFT) within the Quantum ESPRESSO package. The comparison using the GGA-PBE and GGA-PBESol exchange-correlation functionals provided important insights into the effect of chalcogen substitution on the electronic and optical properties of the SnA compounds. The calculated band structures show that SnS is a semiconductor with a narrow direct band gap and SnSe and SnTe are metallic or semi-metallic due to the disappearance of the energy band gap.

The electronic properties are strongly dependent on the atomic size and electronegativity of the chalcogen element, which is evidenced by the steady decrease of the band gap

from SnS to SnTe. The calculated band gaps are underestimated as expected for the conventional GGA approximations and neglecting the spin-orbit coupling effects; however, the obtained trends are physically meaningful and consistent with the previous theoretical reports.Optical studies have also shown that the SnA compounds have a good optical response in the visible and infrared regions. The redshift observed in dielectric spectra and absorption edges from SnS to SnTe confirms an enhancement of low-energy optical activity for heavier chalcogenides. In particular, SnTe exhibited a superior optical conductivity and a more pronounced plasmonic behaviour, whereas SnS showcased promising absorption characteristics for photovoltaic and optoelectronic applications.

Our results suggest that SnS is a promising candidate for the development of semiconductor-based solar energy and optoelectronic devices, whereas SnSe and SnTe may be more suitable for conductive, plasmonic and infrared optoelectronic applications. This work contributes to the theoretical understanding of tin chalcogenides and is a useful reference for future experimental and computational studies to improve their electronic and optical performance by using advanced exchange-correlation methods, inclusion of spin-orbit coupling, alloying or defect engineering.

REFERENCES

Adewale, A. A., Yahaya, A. A., Agbolade, L. O., Yusuff, O. K., Azeez, S. O., Babalola, K. K., Suleman, K. O., Sanusi, Y. K., & Chik, A. (2024). Optoelectronic and mechanical properties of gallium arsenide alloys: Based on density functional theory.

Alsalmi, O., Almuqrin, A. H., Althagafi, T. M., Alharbi, N., Alomairy, S., & Mutlay, I. (2023). *A comparative DFT study of electronic, optical, and thermoelectric properties of Cs2TiBr6 and Cs2TiI6 double perovskites. International Journal of Quantum Chemistry*, 123(9), e27077. https://doi.org/10.1002/qua.27077

Artoni, M., & La Rocca, G. C. (2015). *Parity-time-antisymmetric atomic lattices without gain. Physics Review A,* 91(3)033811. http://doi.org/10.1103/PhysRevA,91.033811

Bafekry, A., Shahrokhi, M., Shafique, A., Jappor, H. R., Fadlallah, M. M., Stampfl, C., Ghergherehchi, M., Mushtaq, M., Feghhi, S. A. H., & Gogova, D. (2021). *Semiconducting chalcogenide alloys based on the (Ge, Sn, Pb) (S, Se, Te) formula with outstanding properties: A first-principles calculation study*. ACS Omega, 6(14), 9433–9441. https://doi.org/10.1021/acsomega.0c06024

Batool, A., Zhu, Y., Ma, X. Saleem, M. I., & Cao, C. (2022). *DFT study of the structural, electronic, and optical properties of bulk, bilayer Sn-monochalcogenides. Advanced Powder Science Advances,* 3, 100275. https://doi.org/10.1016/j.apsadv.2022.100275

Broyden, C. G. (1970)(a). The convergence of a class of double-rank minimization algorithms: I. General considerations. *IMA Journal of Applied Mathematics*, *6*(1), 76–90. https://doi.org/10.1093/imamat/6.1.76.

Broyden, C. G. (1970)(b). The convergence of a class of double-rank minimization algorithms: II. The new algorithm. *IMA Journal of Applied Mathematics*, *6*(3), 222–231. https://doi.org/10.1093/imamat/6.3.222.

Burton, L. A., Colombara, D., Abellon, R. D., Grozema, F. C., Peter, L. M., Savenije, T. J., Dennler, G., & Walsh, A. (2013). *Synthesis, characterization, and electronic structure of single-crystal SnS, Sn_2S_3, and SnS_2. Chemistry of Materials,* 25(24), 4908–4916. https://doi.org/10.1021/cm403046m

Buruiana, A.-T., Mihai, C., Kuncser, V., & Velea, A. (2025). *Advances in 2D Group IV monochalcogenides: Synthesis, properties, and applications. Materials*, 18(7), 1530. https://doi.org/10.3390/ma18071530

Dong, B., Wang, Z., Hung, N. T., Oganov, A. R., Yang, T., Saito, R., & Zhang, Z. (2019). *New two-dimensional phase of tin chalcogenides: Candidates for high-performance thermoelectric materials. Physical Review Materials*, 3(1), 013405. https://doi.org/10.1103/PhysRevMaterials.3.013405

Fatahi, N., Hoat, D. M., Laref, A., Amirian, S., Reshak, A. H., & Naseri, M. (2020*). 2D hexagonal SnTe monolayer: A quasi direct band gap semiconductor with strain sensitive electronic and optical properties. The European Physical Journal B, 93*(32). https://doi.org/10.1140/epjb/e2020-10039-2

Fernandes, P.A. *et al*., *Thermodynamic pathway for the formation of SnSe and SnSe2polycrystalline thin films by selenization of metal precursors, CrystEngComm* 15 (47) (2013) 10278–10286.

Giannozzi, P., Baroni, S., Bonini, N., Calandra, M., Car, R., Cavazzoni, C., Ceresoli, D., Chiarotti, G. L., Cococcioni, M., Dabo, I., Dal Corso, A., de Gironcoli, S., Fabris, S., Fratesi, G., Gebauer, R., Gerstmann, U., Gougoussis, C., Kokalj, A., Lazzeri, M., Martin-Samos, L., Marzari, N., Mauri, F., Mazzarello, R., Paolini, S., Pasquarello, A., Paulatto, L., Sbraccia, C., Scandolo, S., Sclauzero, G., Seitsonen, A. P., Smogunov, A., Umari, P., & Wentzcovitch, R. M. (2009). *QUANTUM ESPRESSO: a modular and open-source software project for quantum simulations of materials. Journal of Physics: Condensed Matter*, 21(39), 395502. https://doi.org/10.1088/0953-8984/21/39/395502

International Energy Agency. (2023). *World Energy Outlook 2023. IEA publications. https://www.Iea.org/world-energy-outlook-2023*

Javed Y., Sikanda M., Mirza, and Rafiz M.A. (2021). *Effect of pressure on mechanical and thermal properties of $SnSe_2$. International journal of thermophysics*, 42,146. https://doi.org/10.1007/s10765-0202894-X

Malon, B.D. E. Kaxiras, *Quasiparticle band structures and interface physics of SnS and GeS, Physical Review* B 87 (24) (2013), 245312

More, M. P., Patil, S. S., & Tayade, R. J. (2023). First-principles investigation of the structural, electronic, optical, thermoelectric properties of Rb2SeTe6 double perovskite material. Materials Science: Materials in Electronics, 34, 164. doi. https://doi.org/10.1007/s10854-023-11147-z

Nabi, M. & Gupta, D.C. "Potential lead-free small band gap halide double perovskites Cs2CuMCl6 (MSb,Bi) for green technology", Scientific Reports 11 (2021) 12945. https://doi.org/10.1038s41598-021-92443-1.

Nwachuku D. N. (2025); First-principles investigation of the electronic structure and optical response of Ga_2S_3 and Ga_2Se_3 chalcogenides, FUDMA Journal of Sciences (FJS), ISSN online: 2616-1370, ISSN print: 2645 – 2944, Vol. 9 No. 11, November, 2025, pp 27 – 31, DOI: https://doi.org/10.33003/fjs-2025-0911-4018.

Pandit, A. & Hamad, B. (2021). *Thermoelectric and lattice-dynamics properties of layered MX (M = Sn, Pb; X = S, Te) compounds. Applied Surface Science*, 538, 147911.

Perdew, J. P., Burke, K., & Ernzerhof, M. (1992). Atoms, molecules, solids, and surfaces: Applications of the generalized gradient approximation for exchange and correlation. *Physical Review B, 46*(11), 6671–6687. https://doi.org/10.1103/PhysRevB.46.6671.

Perdew, J. P., Burke, K., & Ernzerhof, M. (1996). Generalized gradient approximation made simple. *Physical Review Letters, 77*(18), 3865–3868. https://doi.org/10.1103/PhysRevLett.77.3865.

Rajabi, K., Tashakori, H., Pakizeh, E., & Taghizadeh-Farahmand, F. (2025). *First-principles calculations to investigate electronic, optical and thermoelectrical performances of Pb/Te-based nanolayer & bulk chalcogenides. Inter. Journal of Nano Dimension*, 16(1), 1–?

Rundle, J., & Leoni, S. (2022). *Layered tin chalcogenides SnS and SnSe: Lattice thermal conductivity benchmarks and thermoelectric figure of merit. The Journal of Physical Chemistry C,* 126(33), 14036–14046. https://doi.org/10.1021/acs.jpcc.2c02401

Wang, L., Moshwan, R., Yuan, N., Chen, Z.-G., & Shi, X.-L. (2025). *Advances and challenges in SnTe-based thermoelectrics. Advanced Materials*, 37(5), 2418280. https://doi.org/10.1002/adma.202418280

Yahaya, A. A., Yahya, W. A., & Rahmon, I. A. (2024). *Effect of hydrostatic pressure on opto-electronic, elastic and thermoelectric properties of the double perovskites Rb_2SeX_6 (X = Cl, Br): A DFT study. Applied Sciences and Research*, 3(1), Article 171. https://doi.org/10.46481/asr.2024.3.1.171

Yahaya, A. A., Yahya, W. A., Ahmed, A. S., & Sholagberu, A. A. (2024). *Ab initio study of the physical properties of Cs-based double perovskites Cs_2AX_6 (A = Ge, Mn; X = Cl, I). Acta Physica Polonica A,* 145(2), 194–202. https://doi.org/10.12693/APhysPolA.145.194

Yahya, W. A., Yahaya, A. A., Adewale, A. A., Sholagberu, A. A., & Olasunkanmi, N. K. (2023). *A DFT study of optoelectronic, elastic and thermo-electric properties of the double perovskites Rb_2SeX_6 (X = Br, Cl). Journal of the Nigerian Society of Physical Sciences*, 5(2), Article 1418. https://doi.org/10.46481/jnsps.2023.1418

Yue, J., Zheng, J., Li, J., Shen, X., Ren, W., Liu, Y., & Cui, T. (2024). *Characterization of thermoelectric performance in copper-based chalcogenide $CsCu_3S_2$: Unveiling the role of anharmonic lattice dynamics. arXiv*.doi. https://doi.org/10.48550/arXiv.2405.04832

Zhao, G., Zhang, X., Zhang, Y., Sun, X., & Wang, C. (2017). *First-principles study on the structural, electronic and optical properties of Rb_2SeBr_6 under pressure. Journal of Alloys and Compounds*, 728, 1036–1043. https://doi.org/10.1016/j.jallcom.2017.08.110.